SANDIA REPORT

SAND2025-12380 Printed September 2025



MELCOR Deposition Models Applied to Noble Metals

Matthew S. Christian, Troy C. Haskin, David L. Luxat

Prepared by Sandia National Laboratories Albuquerque, New Mexico 87185 Livermore, California 94550 Issued by Sandia National Laboratories, operated for the United States Department of Energy by National Technology & Engineering Solutions of Sandia, LLC.

NOTICE: This report was prepared as an account of work sponsored by an agency of the United States Government. Neither the United States Government, nor any agency thereof, nor any of their employees, nor any of their contractors, subcontractors, or their employees, make any warranty, express or implied, or assume any legal liability or responsibility for the accuracy, completeness, or usefulness of any information, apparatus, product, or process disclosed, or represent that its use would not infringe privately owned rights. Reference herein to any specific commercial product, process, or service by trade name, trademark, manufacturer, or otherwise, does not necessarily constitute or imply its endorsement, recommendation, or favoring by the United States Government, any agency thereof, or any of their contractors or subcontractors. The views and opinions expressed herein do not necessarily state or reflect those of the United States Government, any agency thereof, or any of their contractors.

Printed in the United States of America. This report has been reproduced directly from the best available copy.

Available to DOE and DOE contractors from

U.S. Department of Energy Office of Scientific and Technical Information P.O. Box 62 Oak Ridge, TN 37831

Telephone: (865) 576-8401 Facsimile: (865) 576-5728 E-Mail: reports@osti.gov

Online ordering: http://www.osti.gov/scitech

Available to the public from

U.S. Department of Commerce National Technical Information Service 5301 Shawnee Road Alexandria, VA 22312

Telephone: (800) 553-6847 Facsimile: (703) 605-6900 E-Mail: orders@ntis.gov

Online order: https://classic.ntis.gov/help/order-methods



ABSTRACT

Noble metals are chemically inert elements that form particles that can circulate around the fuel loop of a liquid-fueled molten salt reactor (LF-MSR). Due to their health-hazardous abilities, it is important to track these elements and to understand their contributions to source term during a reaction, particularly for Te as it decays into iodine. This report describes three solid deposition models that were implemented into the MELCOR reactor modeling code. The models that were implemented were Dittus-Boelter for trubulent fluid deposition, Talbot thermophoretic transport equation and Richardson-Zaki gravitational deposition. These closures were used to calculate the mass transfer coefficient and was compared to those reported for the Molten Salt Reactor Experiment (MSRE). The impacts of salt, operation and particle parameters on how they affect solid deposition are described, and found that solid deposition is strongly dependent on salt flow and viscosity, as well as particle diffusion rate and size. The conclusions form the basis for activities to be carried out in FY26 and for pursuit of future activities.

This page intentionally left blank.

CONTENTS

1.	Intro	oduction	11
2.	2.1. 2.2.	RE Observations Salt-Seekers Noble-Gas Daughters Noble Metals	13 13 13 14
3.	3.1.	Physical Phenomenology 3.1.1. Assumptions 3.1.2. Model Objectives Deposition Models 3.2.1. Dittus-Boelter Concentration Flux 3.2.2. Thermophoretic Particle Deposition 3.2.3. Sedimentation 3.2.4. Total Mass Transfer Coefficient Conclusion	17 17 17 18 18 19 19 20 20
4.	4.1. 4.2. 4.3. 4.4. 4.5.	Introduction Mass Transfer Coefficient Dependence on Salt Properties Mass Transfer Coefficient Dependence on Reactor Properties Mass Transfer Coefficient Dependence on Particle Properties Mass Transfer Sensitivity 4.5.1. Dittus-Boelter 4.5.2. Talbot Thermophoretic 4.5.3. Sedimentation 4.5.4. Sensitivity Rates Conclusion	21 21 22 23 24 25 26 26 27 28
5.		Introduction Impact of Noble Metal Species and Particle Size Impact of Temperature Impact of Salt Flow Conclusion	
6	Con	clusion and Future Work	33

References		
------------	--	--

LIST OF FIGURES

Figure 2-1.	Ratio of FPs deposited on surfaces in terms of relative inventory fraction[1]	14
Figure 4-1.	Dependencies of mass transfer coefficient on salt a) density and b) viscosity	21
Figure 4-2.	Dependencies of mass transfer coefficient on salt a) density and b) viscosity	22
Figure 4-3.	Mass Transfer Coefficient vs. Temperature	23
Figure 4-4.	Plot of the diffusion coefficient verses a) particle radius and b) viscosity	23
Figure 4-5.	Mass transfer coefficient vs Diffusion	24
Figure 4-6.	Mass Transfer Coefficient vs. Particle Radius	25
Figure 4-7.	The change in parameter (%) vs change in the Dittus-Boelter mass transfer coefficient (%) for up to a) 100% change and b) 10% change	25
Figure 4-8.	The change in parameter (%) vs change in Tablot thermophoretic mass transfer coefficient (%) for up to a) 100% change and b) 10% change	26
Figure 4-9.	The change in parameter (%) vs change in Richardson sedimentation mass transfer coefficient (%) for up to a) 100% change and b) 10% change	27
Figure 4-10.	Molecular deposition program tree	27
Figure 5-1.	Molybdenum and rhodium mass percent deposition for FLiNaK and FLiBe as a function of time	30
Figure 5-2.	Molybdenum and Rhodium Mass percent deposition at different particle sizes in FLiBe as a function of time	30
Figure 5-3.	Molybdenum mass percent deposition at different temperatures in FLiNaK as a function of time	31
Figure 5-4.	Molybdenum mass percent deposition at different flow rates in FLiNaK as a function of time	31

This page intentionally left blank.

LIST OF TABLES

Table 4-1.	MSRE Parameters Used by Kedl[2]	21
Table 5-1.	MSRE Parameters Reported by Kedl[2] and used in MELCOR MSRE Simulation[3]	29

This page intentionally left blank.

1. INTRODUCTION

A molten salt reactor (MSR) is a non-light water reactor class that uses liquid molten salts as either a coolant or mixed with a liquid salt fuel[4]. The liquid fueled MSR (LF-MSR) circulates a carrier and fissile actinide salt mixture through a primary loop and exchanges heat to a secondary system that is used for either process heat or steam generation[4]. The fuel decay in the primary loop system results in fission product transport across the reactor, which could be released in an accident scenario[3]. The physical form and distribution of the fission products across the reactor will depend on the fission product's chemistry[5]. At any given time during operation, fission products will be present in solid, gaseous or liquid forms. In order to develop operational guidelines for both steady-state and source term release, comprehensive mass transport models must be developed[6, 3].

Although LF-MSR research and development has increased within the last decade, it has focused on the front-end of the molten salt fuel cycle and the chemistry of the higher yield fission products. Fortuitously, most of these fission products remain soluble in the salt, or can be separated via liquid-gas separation processes[7, 2, 5, 8]. However, less attention has been paid to several health hazardous fission products, such as tellurium. Solid "noble metals" (Nb, Mo, Ru, Sb and Te) are reduced to metal form by UF₃ in the fuel salt and are in a metallic state[2]. The salt cannot wet the metal and therefore can migrate to surfaces, where an equilibrium dynamic occurs between adsorption and desorption, and can foul liquid-gas interfaces, such as heat exchangers.

The primary source for benchmarking and validating mass transfer models for LF-MSRs, in the absence of new experiments, benchmarking relies on reports from the Molten Salt Reactor Experiment (MSRE). Although it successfully demonstrated the LF-MSR concept, sampling contamination errors and the era's technology limitations present reported mass balance uncertainties. The fate of noble metals in LF-MSRs largely relies on a singular report by R. J. Kedl, where he applies Dittus-Boelter mass transfer equations to compute mass transfer coefficients for different MSRE components. He then uses those coefficients to develop a reactor based model for noble metal migration and deposition. However, Kedl himself recognizes in his report's conclusion the transferability of his work to other LF-MSR designs.

MELCOR is an integrated systems-level thermal hydraulics and source term code for reactor safety analysis. The code has integrated a number of phenomena required to model non-LWRs and has presented several demonstrations of using the code for non-LWR source term analysis, including three for MSRs[9, 3]. MELCOR is currently revising its modeling approach to provide a "generalized" framework for modeling nuclear facilities. This has given MELCOR an expanded capability to handle a variety of nuclear related activities related to different reactor designs and fuel cycles.

This report details the implementation of solid mass transport closures into MELCOR. Three mass transport closures were chosen to implement into MELCOR that covers turbulent, thermophoretic and gravitational forces, such as the Dittus-Boelter equation studied by Kedl[2]. Although the analysis carried out in this report is concentrated on how the closure relations impact noble metal transport, the generality of the closures can be applied to general mass transport. The report begins by first describing the general chemistry of fission products and the classification. It then details the chemistry and mass transfer of noble metals in Chapter 2. Chapter 3 describes the modeling assumptions required for the closure relationships to apply and their general mathematical formulation. The evaluation of the closures are further explored in Chapter 4. Finally, the report discusses preliminary system results for solid deposition. The report concludes with a discussion of further research and verification efforts as well as future directions for MELCOR development for MSRs.

2. MSRE OBSERVATIONS

The Molten Salt Reactor Experiment (MSRE) was operational from the start of 1966 through 1969. During this time, observations of fission product distribution were noted during and in post-operation sample analysis. In order to decompose the chemical and physical phenomena occurring in MSRE, ORNL simultaneously constructed and performed experiments in a molten-salt convection loop that flowed through the Oak Ridge Reactor (ORR). Together, a well understanding of how most fission products transport and are deposited was generated. This was well summarized in ORNL-4865 and the pertinent observations are summarized below[1]. The description is divided into three types of isotopes: salt-seeking isotopes (Rb, Sr, Y, Zr, Cs, Ba, and rare-earths), noble-gas daughters born from Kr and Xe (Rb, Sr, Y, Cs, Ba) and noble metals (Nb, Mo, Tc, Ru, Rh, Pd, Ag, Cs, In, Sn, Sb, Te and I). Iodine is included as a noble metal as it is born from Te. The noble metal transport can be further subdivided into Nb-Mo-Tc-Ru-Rh-Pd-Ag and Sb-Te-I due to their radionuclide parents.

2.1. Salt-Seekers

The salt seekers primarily travel with the molten salt fluid and are generally well mixed. However, some will always deposit on the surfaces due to fission recoil. Ce, Nb and Zr deposit between 0.001 to 0.003 gram per gram of fuel salt. This results in only 0.1 to 0.2% of salt-seeker isotopes deposited on surfaces within a reactor. The low deposited percentage of salt-seekers on surfaces make these isotopes negligible for deposition immobilization.

2.2. Noble-Gas Daughters

Noble-gas daughters born from Kr are Sr and Y, while Cs and Ba are born from Xe. These metals have similar chemistry to salt-seekers, but have different transport characteristics due to having noble gas precursor. They deposit in greater amounts than salt-seekers because the noble gases impregnate porous solids before decaying into less mobile species. Stripping effectiveness for the noble gases were found to be 68% to 75% effective, resulting in deposition of daughter products in the off gas. Absorbed species were found on surfaces with the ratio of 0.001 to 0.003 grams per gram of MSRE fuel. Due to the unique nature of the deposition mechanism, migration rates for noble metal gases and the daughter species in graphite and metal is required in order to produce the correct transport mechanism.

Table 12.2. Relative deposition intensities for noble metals

	Deposition intensity								
Surface	Flow regime	95 Nb	⁹⁹ Mo	99Tc	¹⁰³ Ru	106 Ru	¹²⁵ Sb	^{129 m} Te	132 T
			Surveilla	nce specin	ens				
Graphite	Laminar Turbulent	0.2 0.2	0.2		0.06 0.04	0.16 0.10		0.15 0.07	
Metal	Laminar Turbulent	0.3 0.3	0.5 1.3		0.1 0.1	0.3			0.9 2.0
			Reactor	compone	nts				
Graphite									
Core bar channel	Turbulent								
Bottom		0.54		0.07		0.25	0.65	0.46 ^a	
Middle		1.09				1.06	1.90	0.92	
Тор		0.23				0.29	0.78	0.62^{a}	
Metal									
Pump bowl	Turbulent	0.26		0.73	0.27	0.38	2.85	0.89^{a}	
Heat exchanger shell	Turbulent	0.33		1.0	0.10	0.19	2.62	1.35 ^a	
Heat exchanger tube	Turbulent	0.27		1.2	0.11	0.54	4.35	2.57 ^a	
Core									
Rod thimble									
Bottom	Turbulent	1.42		1.23	1.54	0.50	3.27	1.65 ^a	
Middle	Turbulent	1.00		0.73	0.58	0.42	1.35	0.54 ^a	

a127Te.

Figure 2-1. Ratio of FPs deposited on surfaces in terms of relative inventory fraction[1]

2.3. Noble Metals

Thermodynamics predicts that noble metal fluorides to not be stable at MSRE's redox potential. In general, the noble metals are believed to be transferred in a mobile separate solid phase within the salt. Deposition of these materials were magnitudes higher than the other fission products, depositing at a rate of 0.1 per gram of MSRE fuel.

Te, Sb and Ag were found to have the most intense deposition rates of all noble metals. Te is unique among the noble metals in that the element has a vapor pressure of 1333 Pa at operating temperature. It is assumed that the gaseous species of the element is a metal particulate and its behavior should be like Xe. Dissolved concentration should be a ratio of 0.0006 for ¹³²Te and 0.00006 for ¹²⁹Te per gram of salt. Te deposition is higher in high flow regions than low flow regions.

Surface deposited Te that decays to iodine was found to desorb back into salt, but Te that diffused into the metal structure and then decayed to iodine remained was immobilized. Observed iodine inventory was 30-60% of the calculated inventory of what was expected to be soluble in the salt, likely because the tellurium precursor was deposited on the surfaces or stripped in the off-gas pump bowl. Therefore, iodine migration and source term is closely tied to the fate of Te.

Niobium is unique and provides an interesting study case. Thermodynamic considerations indicate that at fission product concentration levels, Nb^{4+} is likely to be in equilibrium with niobium metal if the redox potential of the salt is set by U^{3+}/U^{4+} concentration ratios between 0.01 and 0.0001.

Creating a unified deposition model that is representative to all the metal and graphite areas of the system would require knowledge of the effects of flow conditions in each region and the fraction of total area represented by the region. Noble metal deposition is deposited in a fraction of MSRE's

reactor surface area as 26% of the MSRE surface area was metal. Of this, a significant fraction of noble metals was deposited on these surfaces (Figure 2-1).

The bulk of the noble metals remain accessible in the circulating loop but can have varying amounts in circulation at any particular time, however, the total composition is relatively constant. This indicates that the entire inventory is in equilibrium The mobility of the pool of noble-metal material suggests that deposits occur as an accumulation of finely divided well-mixed material rather than as a "plate". Given the spread presented in Figure 2-1 creates difficulty in separating deposition and depletion of different elements on surfaces.

A few percent of noble metals are estimated to has transferred into the off gas, but not through an active transport mechanism. Of those transported to the off-gas, it likely due to the thermophoresis transport of aeresolized noble-metal nano-particles within the pump bowl. Therefore, the primary fission product route in an LF-MSR is likely to be through deposition in the molten salt.

This page intentionally left blank.

3. DEPOSITION MODELS

Creating a unified noble-metal deposition model for MSRs in the absence of verified data is challenging due to little insight on the driving mechanisms. Specifically, there is a lack of information for fate of the different noble metals. Therefore, creating a general model that has the flexibility to expand through addition of necessary physics and chemistry models is required. This chapter defines assumptions for modeling deposition as well as three deposition closure models that have been programmed into MELCOR.

3.1. Physical Phenomenology

3.1.1. Assumptions

The following assumptions are made regarding the system:

- The system is well mixed: At the event modeling time, t = 0, the inventory of noble metals is equally distributed across the MSR. This is supported by evidence of how metals deposited in the MSRE. Assuming this allows an easy set up for radionuclide transport and deposition.
- The reactor is not in a start up condition: In order for the previous condition to be met, the system must have reached a steady state. Additional considerations should be considered for modeling deposition in start-up conditions.
- Mobile metal transport is equal to the salt flow rate during operation: Mass fractions
 between control volumes will be exchanged based on the flow path between the control
 volumes.
- Molecular and gravitational diffusion will dominate when flow is zero: In cases where flow is equal to zero, noble metals will deposit at a rate related to molecular diffusion.

3.1.2. Model Objectives

The following are targets for model implementation that define success criteria:

• A fraction of noble-metals is "deposited" by being "held" in the control volume: Deposited fission product mass is represented by subtracting mass from the "floating pool" of fission products that is being transferred between control volumes.

- A fraction of noble-metals is "depleted" by being "returned" to the pool after undergoing decay. Each metal has different adsorption interactions with metal surfaces, particularly with metals Nb, Mo, Tc and Ru. Some metals may deposit as Mo but then be depleted after decaying to Ru. Thermal effects will also contribute to desorption.
- A chemistry model niobium is required: The chemical state of Nb as Nb⁴⁺ or Nb⁰ depends on the environment's redox condition. Any present Nb⁴⁺ would not be available for deposition. Additionally, system redox changes will deplete and re-mobilize deposited Nb.
- An iodine fraction needs to be represented as deposited in on metal: Strongly absorbed Te in metal decays and was a sink for iodine. However, a fraction of deposited iodine will desorb and return to the pool.

3.2. Deposition Models

The following describes the different models that are used to calculate solid deposition. Each model will have contributions under different circumstances and are discussed from slower to larger flow conditions.

3.2.1. Dittus-Boelter Concentration Flux

This mass transfer method combines diffusive and convective mass transport deposition mechanisms related to the dimensionless Reynolds (Re) and dimensionless Schmidt number (Sc):

$$Re = \frac{\rho_l U_l L}{\mu_l} \tag{3.1}$$

$$Sc = \frac{\mu_l}{\rho_l D_p} \tag{3.2}$$

Here, ρ_l is the liquid density, U_l is the fluid velocity, L is the characteristic length, taken as the pipe diameter, μ_l is the fluid viscosity and D_p is the particle diffusion coefficient. In the absence of known diffusion coefficients, we use the Stokes-Einstein-Sutherland diffusion coefficient.

$$D_p(m^2/s) = \frac{k_B T_l}{6\pi\mu_l r_p} \tag{3.3}$$

where k_B is the Boltzmann constant, T_l is the system temperature and r_p is the particle radius. The transfer coefficient, k_{DB} , is therefore:

$$k_{DB}(m/s) = 0.023 \frac{D_p}{L} Re^{0.8} Sc^{0.4}$$
 (3.4)

The differentiable rate of mass deposition by molecular diffusion is:

$$\frac{dC}{dt}(kg/m^3 \cdot s) = \frac{1}{V}k_{DB}A(C_B - C_S)$$
(3.5)

where A is the surface area, C_B is the bulk concentration and C_S is the surface concentration in mass/ m^3 . This is the deposition model was proposed by Kedl[2] to model noble metal deposition in MSRE and has been implemented in CTF by Sam Walker[10].

3.2.2. Thermophoretic Particle Deposition

Thermophoretic mass transfer depends on two dimensionless numbers that depict the mass transfer gradient from the thermal energy flux (Dufour number) and the temperature gradients on concentration distributions (Soret number)[11]. A first order approximation for thermophoretic mass transfer can be made by using Talbot $et\ al$'s approximation for the thermophoretic mass transfer coefficient[12] that depends on the Knudsen number, Kn:

$$Kn = \frac{\mu_l}{\rho_l L} \sqrt{\frac{m_p \pi}{2k_B T_l}} \tag{3.6}$$

where m_p is the particle mass. The thermophoretic mass transfer coefficient, k_T can be defined as:

$$k_T = \frac{2C_1\mu_l(\frac{k_l}{k_p} + C_2Kn)}{L\rho_l T_l(1 + 2C_3Kn)(1 + 2\frac{k_l}{k_p} + 2C_4Kn)} \nabla T$$
(3.7)

where k_l and k_p are the thermoconductivity of the liquid and particle. The term ∇T is the temperature gradient and in this context is defined as the difference between the salt temperature and the surface (heat structure). The constants C_1 , C_2 , C_3 and C_4 are constants that are fitted to a system on the order of unity. In the instance that the thermoconductivity of the particle and liquid are close and the system parameters are unknown, a good approximation is:

$$k_T = \frac{2\mu_l(1 + Kn)}{L\rho_l T_l(1 + 2Kn)(3 + 2Kn)} \nabla T$$
(3.8)

The differentiable rate of mass deposition has a similar form as the molecular diffusion deposition, but does not depend on the deposited mass deposition.

$$\frac{dC}{dt}(kg/m^3 \cdot s) = \frac{1}{V}k_T A C_B \tag{3.9}$$

3.2.3. Sedimentation

In the absence of flow, Dittus-Boelter deposition will go to zero and thermophoretic and gravitational forces will dominate deposition. Because the concentration of noble metals will be dilute in the reactor, particles will not have a packing order during deposition and using Richardson and Zaki's formula[13], the deposition velocity will be equal to the particle's terminal velocity:

$$v_s(m/s) = \frac{d_p^2(\rho_p - \rho_l)g}{18\mu_l}$$
 (3.10)

where d_p is the particle diameter and ρ_p is the particle density. Similarly, the differentiable concentration difference can be expressed as:

$$\frac{dC}{dt}(kg/m^3 \cdot s) = \frac{1}{V}v_s A C_B \tag{3.11}$$

3.2.4. Total Mass Transfer Coefficient

Mass transfer coefficients are additive and can be expressed as a sum. Therefore, the total mass transfer coefficient, k_t , can be expressed as:

$$k_t = k_{DB} + k_T + v_s (3.12)$$

3.3. Conclusion

In this chapter, we introduced the background for modeling noble particle deposition in MELCOR as well as the assumptions required for modeling particle deposition. We then describe three closures chosen to represent turbulent, thermophoretic and gravitational particle deposition that was implemented into MELCOR. The following chapter describes how the mass transfer coefficient for these closures change with salt, reactor and particle properties.

4. CLOSURE EVALUATION

4.1. Introduction

This chapter explores how the closure relationships discussed in the previous chapter vary with system parameters. The identified key dependent parameters relate to salt properties (salt density and viscosity) reactor properties (flow velocity, characteristic length and fluid temperature) and particle properties (diffusion coefficient and particle radius). We also compare the Dittus-Boelter mass transfer coefficient using both the Stokes-Einstein-Sullivan (SES) approach for calculating diffusion coefficients and Kedl's static particle diffusion coefficient (K). We use a base case of the parameters reported in Table 4-1, varying one parameter at a time. The chapter also explores sensitivities of the closures by illustrating the percent change of mass transfer with percent change in parameter.

Table 4-1. MSRE Parameters Used by Kedl[2]

$\rho_l(kg/m^3)$	$\mu_l(mN \cdot s/m^2)$	U(m/s)	L(m)	T(K)	$D(m^2/s)$
2,245	0.0078	5.96	0.127	923	$5.1 \cdot 10^{-9}$

4.2. Mass Transfer Coefficient Dependence on Salt Properties

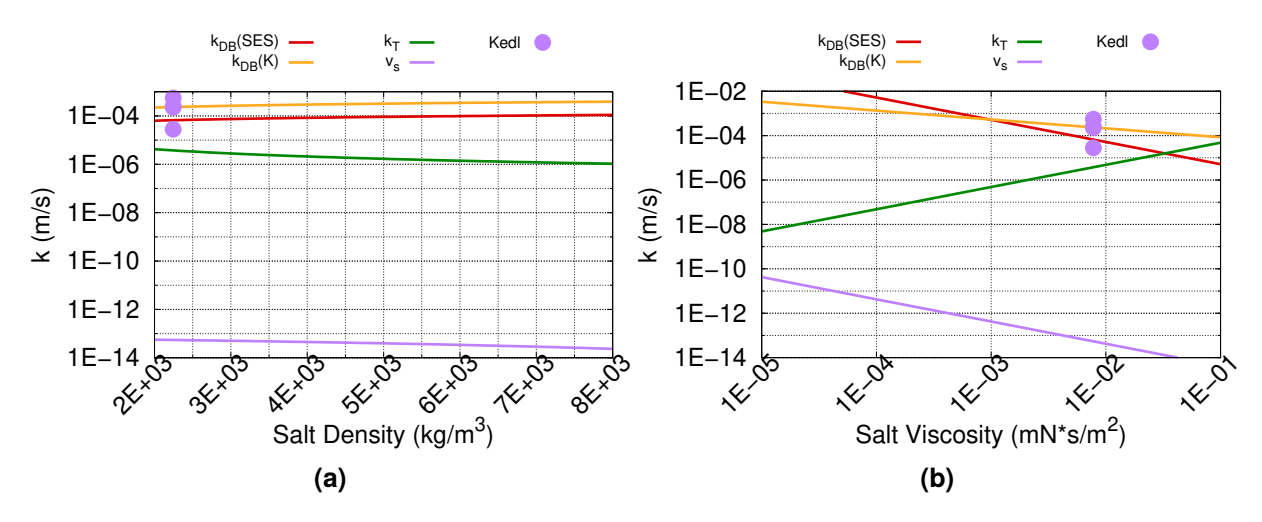


Figure 4-1. Dependencies of mass transfer coefficient on salt a) density and b) viscosity.

Figure 4-1a shows how the mass transfer coefficients change with salt density for Dittus-Boelter $(k_{DB}(SES), k_{DB}(K))$, Talbot (k_T) and Richardson-Zaki (v_s) . Kedl's mass transfer coefficients

are also plotted. Both Dittus-Boelter plots agree well with Kedl's report, though using Ked'ls reported diffusion coefficient results in higher mass transfer. Overall, Dittus-Boelter has as a smaller dependence on salt density for mass transfer than thermophoretic and gravitational solid transport mechanisms. Thermophoretic mass transport increases inversely proportional to salt density. Although Figure 4-1a is bound at $2,000 \, kg/m^3$, the thermophoretic mass transfer coefficient surpasses Dittus-Boelter at low viscosities. It also varies less at higher densities. Although there is a density dependence for Richardson-Zaki sedimentation, the magnitude of the change is washed out by the small particle diameter used in these calculations.

Figure 4-1b shows that viscosity has a greater affect on mass transfer coefficient than salt density. Dittus-Boelter mass transport decreases with increasing viscosity. Kedl's and the Stokes-Einstein-Sullivan crosses at $0.001 \ mNs/m^2$ due to the dependent of the diffusion coefficient on viscosity. Thermophoretic mass transfer increases with salt viscosity and eventually crosses Dittus-Boelter transport. Richardson-Zaki sedimentation decreases at a similar rate as Dittus-Boelter (SES). Again, the magnitude of mass transfer for Richardson-Zaki is lower due to the particle size.

4.3. Mass Transfer Coefficient Dependence on Reactor Properties

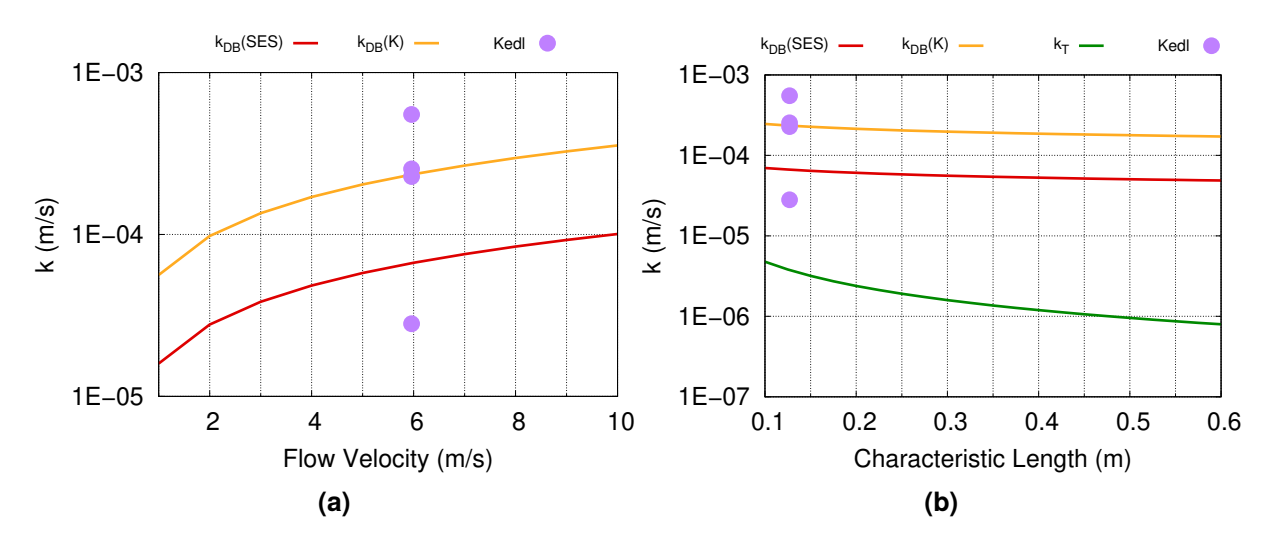


Figure 4-2. Dependencies of mass transfer coefficient on salt a) density and b) viscosity.

Only Dittus-Boelter has a dependence on fluid flow, which contributes to the Reynolds number. The mass transfer has greater changes at flow velocities below $4 \, m/s$ than at higher velocities. Figure 4-2a shows how diffusion coefficient changes the magnitude of Dittus-Boelter mass transport. Characteristic length has the same relationship with fluid flow velocity, but has a smaller effect on mass transport compared to flow velocity. Thermophoretic mass transport decreases with characteristic length. Overall, flow velocity and characteristic length, for MSRE parameters have less effects than salt properties.

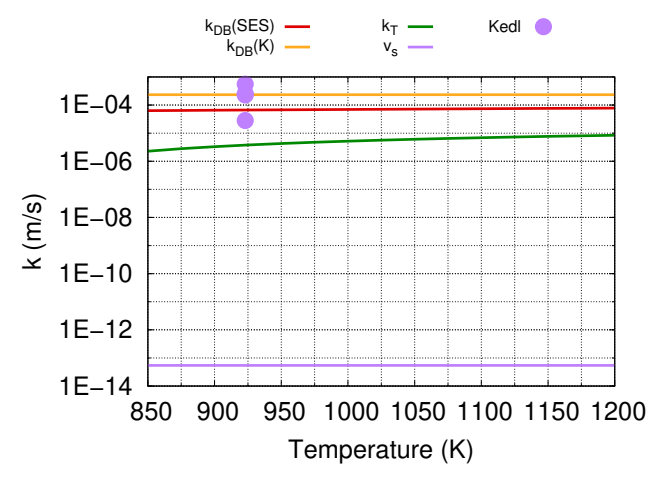


Figure 4-3. Mass Transfer Coefficient vs. Temperature

4.4. Mass Transfer Coefficient Dependence on Particle Properties

The diffusion coefficient plotted as a function of particle radius is shown below in Fiugre 4-4a. The assumed conditions are of those reported by MSRE and are reported in Table 4-1. Kedl used a diffusion coefficient of $5.1 \cdot 10^{-5} m^2/s$ for all noble metals and under all conditions. Neither the derivation nor a citation for this value was noted. This results in a back calculated radius smaller than 1.0.

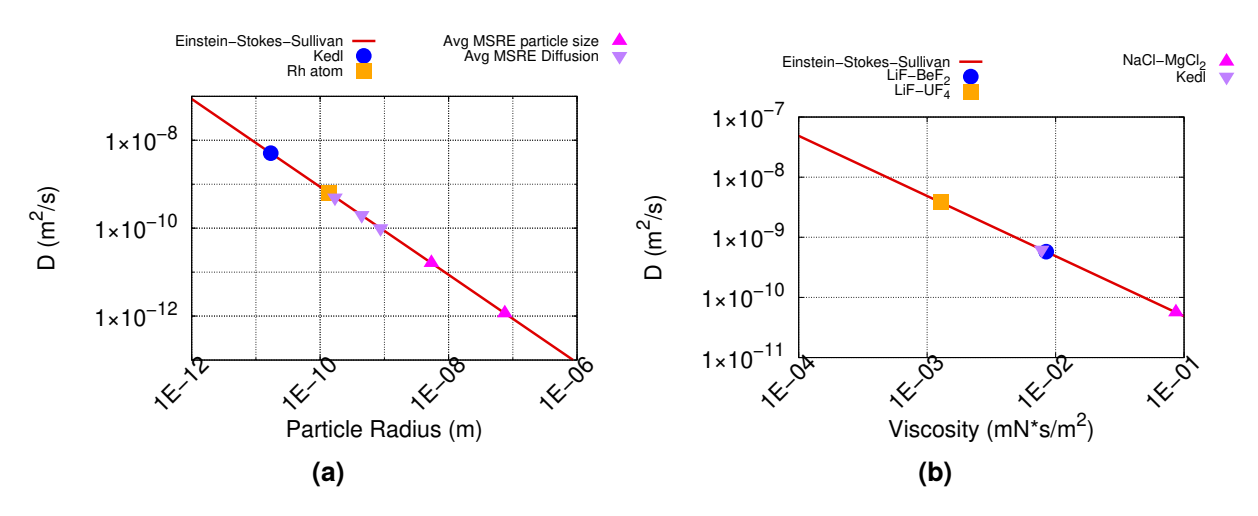


Figure 4-4. Plot of the diffusion coefficient verses a) particle radius and b) viscosity.

Smaller diffusion coefficients were reported for species in salts, such as for uranium $(2 \cdot 10^{-10} m^2/s)$, $Cr^{2+} (5 \cdot 10^{-10} m^2/s)$ and $BF_3 (1 \cdot 10^{-10} m^2/s)[14]$. Average reported particles sizes of noble metals were also plotted for 54Å and 750Å which would yield lower diffusion coefficients[15]. The calculated diffusion coefficient using rhodium's atomic radius is similar to those calculated for chromium and uranium, indicating that using the Einstein-Stokes-Sullivan equation using atomic radii is appropriate.

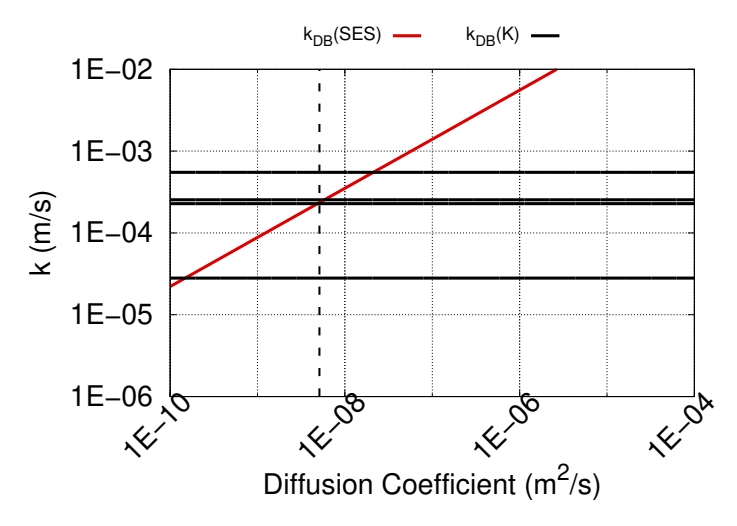


Figure 4-5. Mass transfer coefficient vs Diffusion

Illustrating the importance of Dittus-Boelter mass transfer coefficients is illustrated in Figure 4-5, which shows how k_{DB} varies with diffusion coefficient and the reported mass transfer coefficients by Kedl. The diffusion coefficient used by Kedl is also plotted. The graph shows the intersections of Kedl's diffusion coefficient and mass transfer coefficients, which correspond to the heat exchanger shell and the core wall cooling annulus. The diffusion coefficient must change in order for Dittus-Boelter to reproduce Kedl's mass transfer coefficient and will be supported as the only parameter that can change to accommodate the wide values is the diffusion coefficient

The diffusion coefficient as a function of viscosity for a rhodium are plotted in Figure 4-4b for the Stokes-Einstein-Sullivan equation in addition to points for Kedl's used salt viscosity and other 50:50 binary salt compositions that were obtained from the Molten Salt Thermodynamic Database (MSTDB-TP)[16]. The results show that the mobility of radionuclides in salts will increase as viscosity decreases.

Figure 4-6 shows how dependent the total mass transfer coefficient is on particle size. At the small particle sizes, 35-180 Å solid mass transfer in MSRE is dominated by Dittus-Boelter. At larger particle sizes, 1,000-2,000 Å mass transport is a combination of Dittus-Boelter and thermophoretic mass transfer processes. Above one micron, solid mass deposition is dominated by gravitational driven processes.

The previous results have shown how dependence of particle radius and in-turn particle diffusion contribute to solid-liquid mass transport. The results show, and will be further substantiated in the following section, that accurate knowledge of particle diffusion and particle size are important for determining solid transport and deposition.

4.5. Mass Transfer Sensitivity

This section provides a parameter sensitivity analysis for the three implemented mass transfer closures. The sensitivity is expressed as the change in model parameters plotted against the change in mass transfer coefficient, both in units of percent change. The sensitivity is illustrated in up to

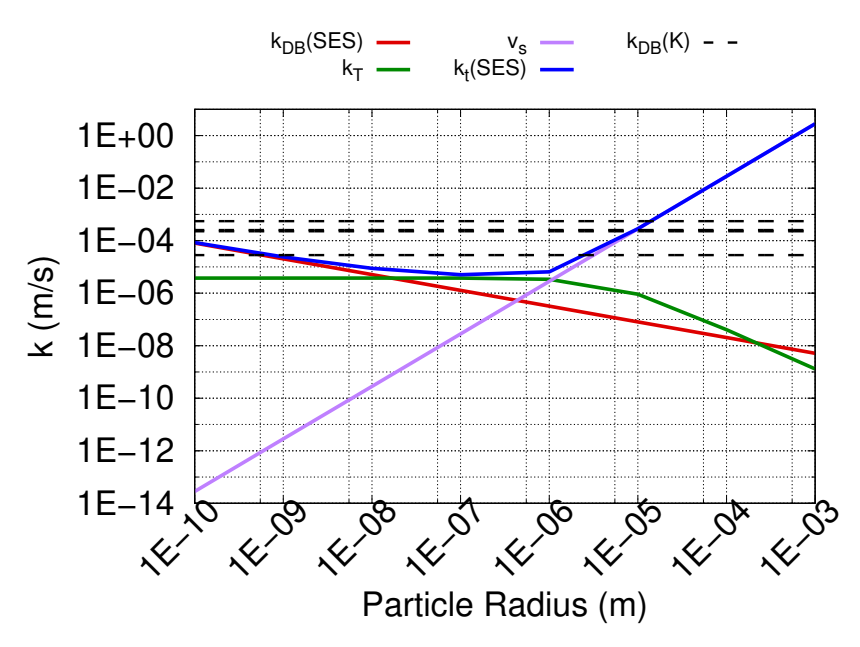


Figure 4-6. Mass Transfer Coefficient vs. Particle Radius

100 % change, and second graph up to 10% change to illustrate "chemical accuracy". In order to illustrate how quick the sensitivity changes, the slope of the sensitivity if plotted as a bar graph and identifies the MSR properties that result in the largest changes in mass transfer and therefore need better understanding.

4.5.1. Dittus-Boelter

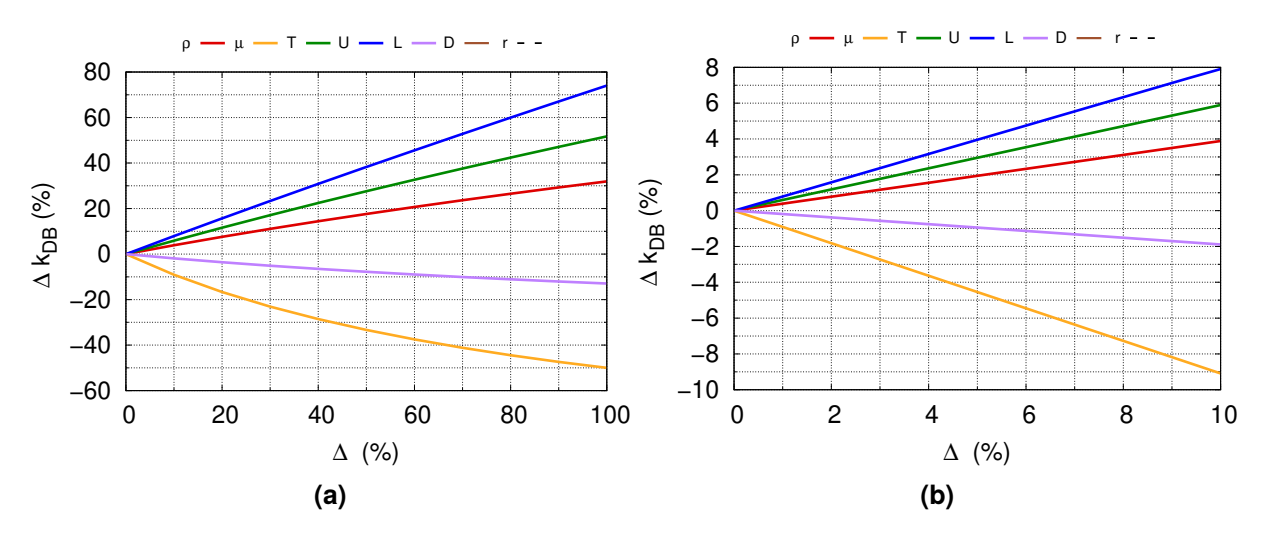


Figure 4-7. The change in parameter (%) vs change in the Dittus-Boelter mass transfer coefficient (%) for up to a) 100% change and b) 10% change.

Figure 4-7 shows the sensitivity of Dittus-Boelter to salt density, flow, temperature and viscosity, in addition to particle diffusion and radius and characteristic length. The results in Figure 4-7a shows that doubling the flow velocity can change mass transfer up to 80%. Salt viscosity and

temperature also have large effects from property doubling, changing by 40% Temperature and particle diffusion are equal, as temperature directly affects particle diffusion. Although doubling Dittus-Boelter parameters has up to 80% for mass transfer effect. However, Figure 4-7b shows that if Dittus-Boelter parameters are known within 10%, then Dittus-Boelter mass transfer coefficients will likewise be able to achieve chemical accuracy.

4.5.2. Talbot Thermophoretic

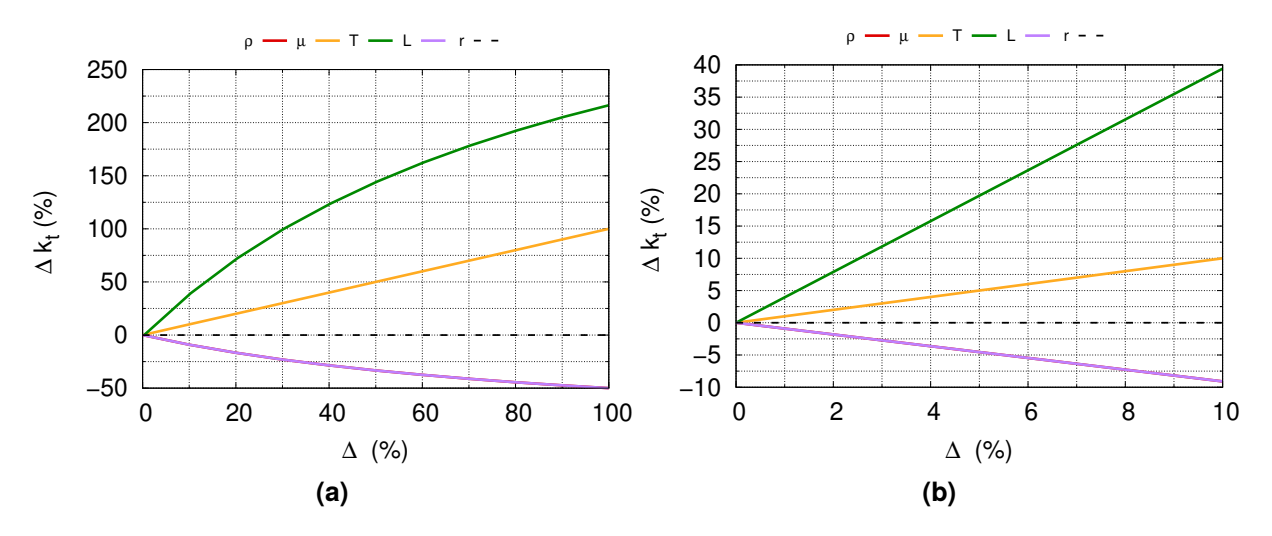


Figure 4-8. The change in parameter (%) vs change in Tablot thermophoretic mass transfer coefficient (%) for up to a) 100% change and b) 10% change.

Figure 4-8 shows that doubling dependent parameters can have up to a 225% increase in thermophoretic mass transport. Not surprisingly, temperature has the largest effect on mass transport. Although we plot temperature change, the driving phenomena for thermophoretic mass transfer is the temperature gradient, making the possibility of achieving such changes plausible in MSRs. Salt viscosity also shows similar effects on mass transfer as Dittus-Boelter. A doubling of salt viscosity doubles thermophoretic mass transfer. Change in particle radius has little effect on thermophoretic mass transport, as the particle density will largely change. Figure 4-8b shows that the temperature gradient must be known within 2% must be known in order to have a thermophoretic mass transport coefficient to be no more than 10%. Characteristic length shows a 1:1 change. However, characteristic length is typically assumed to be pipe diameter and will have low uncertainty in reactor design. Salt viscosity is within the acceptable limits.

4.5.3. Sedimentation

Figure 4-9 shows the sensitivity of gravitational settling to salt density and viscosity, and particle radius vs mass transfer coefficient. The results shows that particle size is strongly dependent for gravitational deposition, resulting in a 300% increase with a doubling of particle size (Figure 4-9a). A 50% reduction in transport is achieved with doubling of salt viscosity.

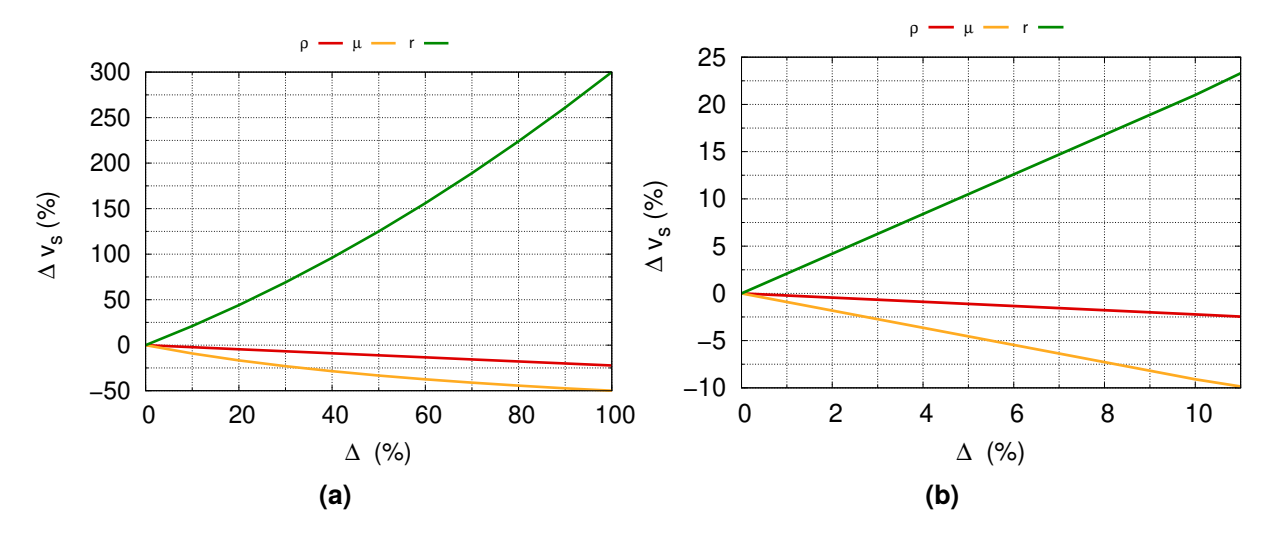


Figure 4-9. The change in parameter (%) vs change in Richardson sedimentation mass transfer coefficient (%) for up to a) 100% change and b) 10% change.

4.5.4. Sensitivity Rates

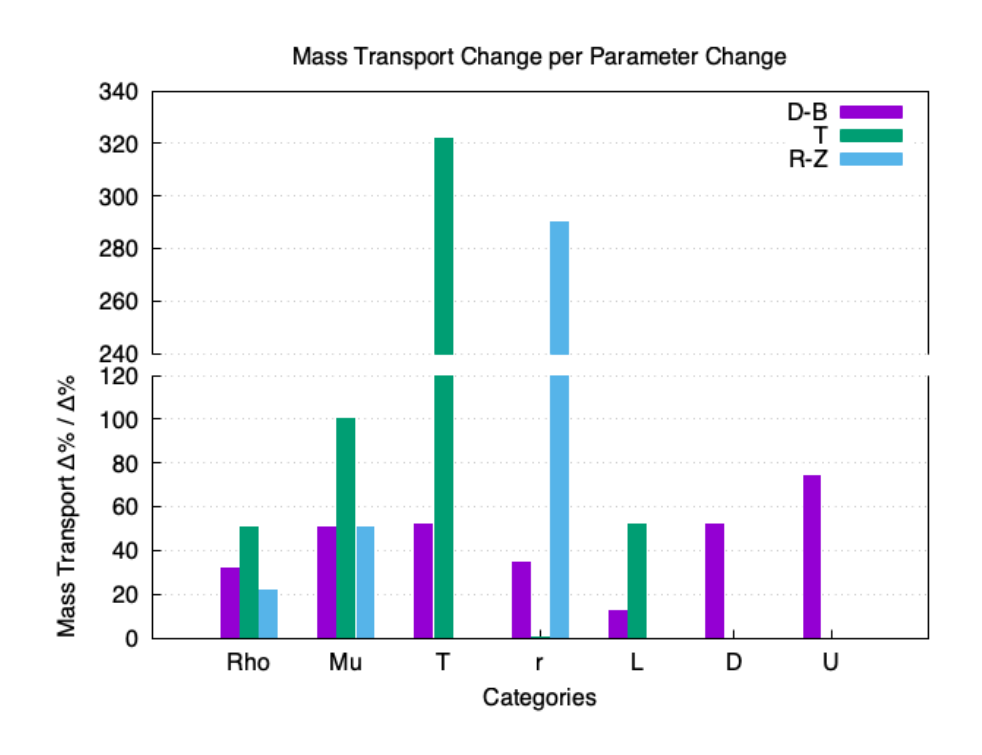


Figure 4-10. Molecular deposition program tree.

The slopes of the lines in Figures 4-7, 4-8 and 4-9 are plotted in figure 4-10 and depict the percent change in solid deposition for every percent change in parameter, i.e., for every percent change in salt flow velocity, there will be a 65% change in the Dittus-Boelter mass transfer coefficient. The graph highlights the parameters that drive changes in the three closures implemented for solid

deposition. Salt flow, salt viscosity and temperature have equal effects on Dittus-Boelter mass transfer quantities as particle diffusion. However, flow conditions will change this closure the greatest and follows observations from MSRE (Figure 2-1) where the greatest deposition occurred in turbulent flow regimes and thus where the Reynold's number would be high.

As expected, temperature strongly drives thermophoretic mass transfer, having a 320% change in mass transfer for each percent change in temperature. In general, each property that construct's Talbot's thermophoretic has high changes for mass transfer coefficient. Similarly, particle radius drives gravitational settling, with salt density having the least effect.

Ranking the parameters in in Figure 4-10 on the drivers for solid deposition will be properties of the particle (particle radius and diffusion) as well as system properties (salt flow and temperature). Salt viscosity also can have a significant effect, while salt density and Characteristic length had the least effects.

4.6. Conclusion

This chapter carried out analysis of how mass transfer coefficients for the DIttus-Boelter, Talbot and Richardson-Zaki equations are influenced by salt properties (density, viscosity, and temperature), design components (salt flow and pipe diameter), and particle properties (difussion rate and size). The Dittus-Boelter coefficient exhibited a less dependence on salt density compared to thermophoretic and gravitational transport, with thermophoretic mass transfer inversely related to salt density. Viscosity was found as a key parameter, as Dittus-Boelter mass transport declines with increasing viscosity. The interplay between diffusion coefficients and particle sizes underscores the necessity for better understanding of solid-liquid mass transport processes. Smaller particle sizes primarily deposit via Dittus-Boelter equations, whereas larger sizes will be dominated by gravitational forces. Overall, the mass transport coefficients are less than those of Kedl's, who used a higher particle diffusion coefficient than those reported elsewhere in MSRE literature.

Parameter sensitivity analysis for the three mass transfer closures revealed that changes in flow velocity, salt viscosity, and temperature can lead to significant variations, with flow velocity causing up to an 80% change in mass transfer. The temperature gradient is influential in thermophoretic mass transfer, where a doubling of temperature can result in a 320% increase in mass transport. Accurate knowledge of parameters such as temperature and characteristic length is essential for achieving chemical accuracy in mass transfer coefficients. Notably, particle size significantly affects gravitational settling, with a doubling of particle size leading to a 300% increase in mass transfer. The analysis ranks the parameters influencing solid deposition, highlighting the importance of particle properties (radius and diffusion) and system properties (salt flow and temperature), while noting that salt viscosity also plays a significant role, and salt density and characteristic length have a lesser impact. Overall, these findings emphasize the need for a comprehensive understanding of these parameters to best model solid-liquid mass transport processes in molten salt reactors.

5. ANALYTICAL SIMULATION RESULTS

5.1. Introduction

This chapter explores the time-evolution of noble metal solid deposition in molten salts with temperature dependent salt properties (density and viscosity). The effect of particle size, element species and flow rate are also explored. Although the closures in the previous chapters have been implemented into MELCOR, the current software development state of generalized MELCOR only provides categorical unit testing, providing no ability to model full reactor systems. This means that the radionuclide transport software class is not connected to models for a reactor core or the salts equation of state. The capability to do full reactor analysis is expected to be completed in FY26. In order to analyze the the afore mentioned parameters on deposition, we we use the analytical rate equations described in Chapter 3.

Each section uses the same base parameters of those in Chapter 4 and are reported again in Table 5-1. The species selected for analysis are molybdenum and rhodium, and use their respected densities and atomic radii. The salts chosen for analysis are FLiNaK and FLiBe, and use reported temperature relationships for density and viscosity. Control volumes and surface areas were taken from CV310 from MELCOR's MSRE demonstration[3]. This CV connects the gas stripper to the heat exchanger and is a representitive pipe section of the MSRE. A concentration of 0.1 kg of starting product was chosen, which relates to approximately 50 ppm concentration. Results are reported in terms of mass percent deposited on the surface as a function of minutes.

Table 5-1. MSRE Parameters Reported by Kedl[2] and used in MELCOR MSRE Simulation[3]

Element	r	$\rho_p (kg/m^3)$	L(m)	U (m/s)	T(K)	$V(m^3)$	$A(m^2)$	$C_B(kg)$
Mo	1.39	10,220	0.127	5.98	022	$3.24 \cdot 10^{-3}$	0.20	0.1
Rh	1.35	12,310	0.127	3.96	923	3.24.10	0.30	0.1

5.2. Impact of Noble Metal Species and Particle Size

Figure 5-1 shows molybdenum and rhodium in FLiNaK and FLiBe mass percent deposited over time. The differences between the salt compositions are not apparent until 20 minutes. FLiBe has higher solid deposition of both species than FLiNaK. Within each salt, there is negligible difference between molybdenum and rhodium, where rhodium has greater mass transfer than molybdenum.

Figure 5-2 shows the mass percent deposited for different particle sizes. Using atomic radii as the particle sizes results in deposition above 20% verses the smaller percentage when using noble metal particle sizes reported in MSRE. The deposited mass percent drops to 2% when using a radius

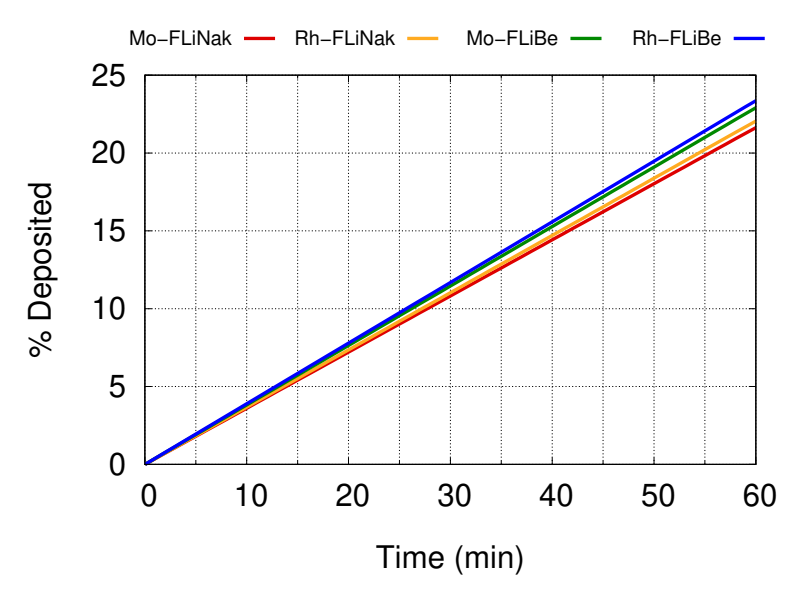


Figure 5-1. Molybdenum and rhodium mass percent deposition for FLiNaK and FLiBe as a function of time

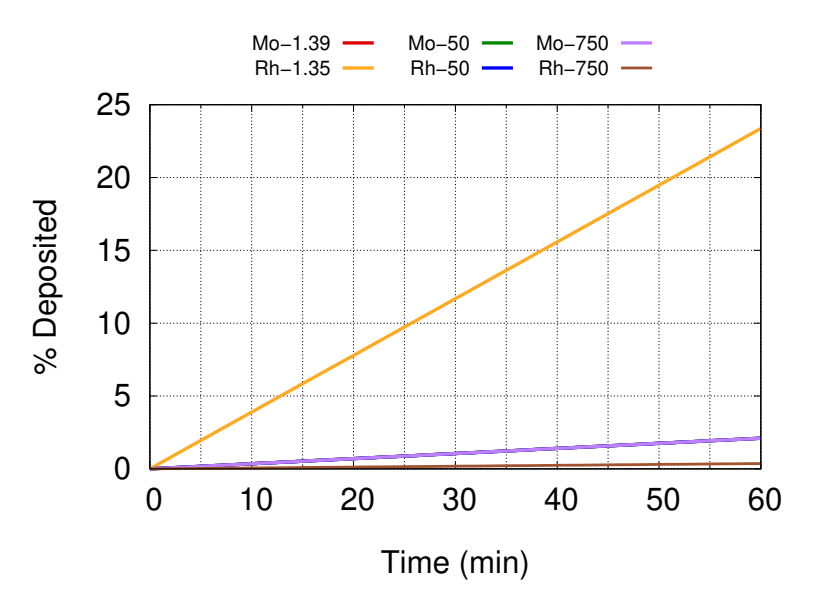


Figure 5-2. Molybdenum and Rhodium Mass percent deposition at different particle sizes in FLiBe as a function of time

of 50Å and down to 1% when using the larger radii of 750ÅThere is also no distinguish between molybdenum and rhodium at larger particles. We will therefore no longer distinguish between element type on the next sections and assume modeling of a 50Å radius particle.

5.3. Impact of Temperature

Figure 5-3 shows the temperature effects for mass percent deposition for 50Å molybdenum particles in FLiNaK. The 923K represents MSRE. Reducing the temperature by 50K reduces the deposited

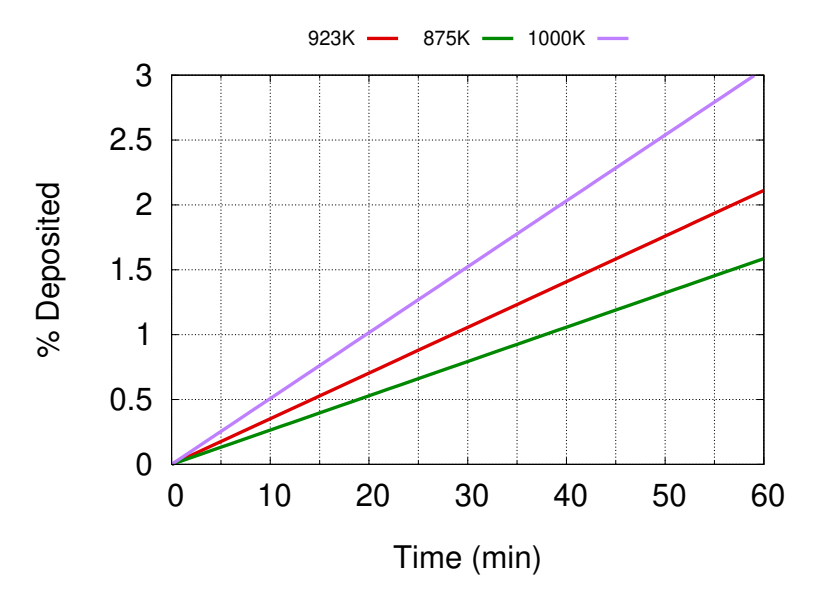


Figure 5-3. Molybdenum mass percent deposition at different temperatures in FLiNaK as a function of time

mass percent by 0.5 % while increasing the temperature by 78K increases the rate by 1%. As temperature increases, the diffusion rate of the particle increases. However, salt density and viscosity decreases and also affect the movement of the a particle to a surface. Temperature will therefore be a driver for deposition of noble metals.

5.4. Impact of Salt Flow

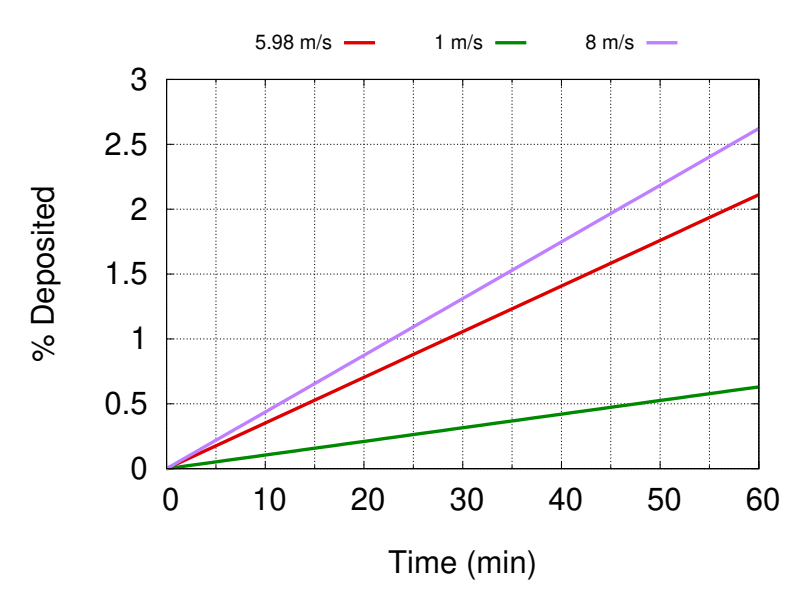


Figure 5-4. Molybdenum mass percent deposition at different flow rates in FLiNaK as a function of time

Figure 5-4 shows the effect of pump flow rate for 50Å molybdenum particles in FLiNaK at 923K.

As mentioned in the previous chapter, the salt flow rate is a parameter only in the the Dittus-Boelter mass transfer coefficient and will not affect thermophoretic or gravitational deposition models. Raising the salt flow rate from MSRE conditions to 8 m/s raises the deposition rate by 0.5 %, while lowering the flow rate to 1 m/s will lower the mass percent to 0.6 % per hour. This reflects observations from MSRE that showed higher solid deposition in turbulent regimes.

5.5. Conclusion

In this chapter, we looked at the system level for mass percent deposition of noble metals in FLiNaK and FLiBe molten salts. The results are in line with those of the previous chapter, showing that slat temperature and flow, and particle size will drive the deposition of noble metals. However, the small differences for molybdenum and rhodium show that using a uniform diffusion coefficient based on particle size does not result in any data loss when the particle size reaches a certain threshold. The particle size had the greatest affect on solid mass deposition, as increasing the particle radius from an atomic radius to MSRE observed particle radius significantly decreased the mass percent transfer.

6. CONCLUSION AND FUTURE WORK

This report discusses noble metal deposition and associated modeling approaches in liquid fueled molten salt reactors (LF-MSRs). The discussed closures have been implemented into the MELCOR nuclear reactor model code to model their circulation and deposition. The report investigates the sensitivities of the implemented closures with reported data from the Molten Salt Reactor Experiment (MSRE) and also investigates the sensitivity of the mass percent deposition for several parameters

Noble metals, such as molybdenum and rhodium, are expected to circulate around the fuel loop, but differ from other fission products due to their chemical inertness. The mass balance of those deposited on surfaces is unknown, but most deposition occurs on metal surfaces. Deposition processes are in equilibrium with particle desorption. However, some noble metals are expected to adhere to bubble surfaces and transfer via bubbles. Mechanisms for off-gas system transfer are likely to adhere to these mass transfer systems.

The work highlighted here is the first step in adding solid deposition mechanisms in generalized MELCOR. Three approaches were implemented to capture turbulent, thermophoretic and gravitational solid deposition. These approaches have been used by others for modeling solid deposition of noble metals and can be used to model other depositional processes, such as for aerosols. Sensitivity analysis showed that salt temperature and flow rate will drive noble metal deposition. Salt-choice will also affect depositional processes, as more dense and viscious salts will have less solid deposition.

Particle characteristics diffusion and size were shown to be the largest deposition driver. A method tor estimate particle size distribution within the reactor must be created and is a planned FY26 activity. Additionally, a desorption mechanism must be implemented to release noble metals back into the salt to create the equilibrium steady-state condition described by MSRE reports[2, 1]. The closures implemented in MELCOR's radionuclide package are planned to be connected to core and equation of state packages in FY26 to provide a more comprehensive view of noble metal desorption. Additional identified closures to be implemented in MELCOR include bubble transport and sticking probably. Bubble transport mechanisms will be implemented into MELCOR in FY26, but require known sticking coefficients that are to be determined.

Finally, the results presented here are computed from analytical equations. The data used to benchmark these models in MSRs come from a singular report by Kedl, who had serious reservations for scaling his analysis to different reactor designs. The used diffusion coefficient for noble metal particles were higher than estimated diffusion coefficients for atom sized particles. The use of the reported diffusion coefficient will result in higher solid mass deposition. We therefore reiterate some experimental recommendations made concluding Kedl's report to be studied in a salt circulation loop[2]:

- Deposition on solid surfaces and correlation of results with mass transfer theory.
- Deposition on liquid-gas interfaces and correlation of results with mass transfer theory.
- Stabilizing effects of noble metals (fission products and corrosion products) on bubble and foam interfaes.
- Effects of the chemical state of the salt.
- Interaction of noble metals with bubbles.

This would lay the foundation for increasing the accuracy of the solid deposition mass transfer theory in molten salts that could be used to be compared to an actual LF-MSR.

REFERENCES

- [1] E. G. Bohlmann F. F. Blankenship W. R. Grimes E. L. Compere, S. S. Kirsilis. Fission product behavior in the molten salt reactor experiment. Technical report ORNL-4865, Oak Ridge National Laboratories, May 1975.
- [2] R. J. Kedl. The migration of a class of fission products (noble metals) in the molten salt reactor experiment. Technical report ORNL-TM-3884, Oak Ridge National Laboratories, May 1972.
- [3] Troy Haskin David Luxat Rod Schmidt Kenneth Wager, Brad Beeny. Melcor accident progression and source term demonstration calculations for a molten salt reactor. Technical report SAND2023-01803, Sandia National Labortories, May 2023.
- [4] Status of Molten Salt Reactor Technology. Number 489 in entity. INTERNATIONAL ATOMIC ENERGY AGENCY, 2023.
- [5] R. Thoma. Chemical aspects of msre operations. Technical report ORNL-4658, Oak Ridge National Laboratories, May 1971.
- [6] D. Holcomb et al. Early phase molten salt reactor safety evaluation considerations," oak ridge national labortory. Technical report ORNL/TM-2020/1719, Oak Ridge National Laboratories, May 2020.
- [7] W. R. Grimes. Radiation chemistry of msr system. Technical report ORNL-TM-500, Oak Ridge National Laboratories, May 1963.
- [8] Theodore Besmann et al. Applications of thermochimical modeling in molten salt reactors. *Materials*, 17:495, 2024.
- [9] Bradley Beeny Fred Gelbard Kenneth Wagner, Troy Haskin and David Luxat. Melcor accident progression and source term demonstration calculations for a fhr. Technical report SAND2022-2751, Sandia National Laboratories, Albuquerque, New Mexico 87185 and Livermore, California 94550, May 2023.
- [10] Samuel A. Walker and Wei Ji. Species transport analysis of noble metal fission product transport, deposition, and extraction in the molten salt reactor experiment. *Annals of Nuclear Energy*, 158:108250, 2021.
- [11] Jean K. Platten. The soret effect: A review of recent experimental results. *Journal of Applied Mechanics*, 73:5–15, 2005.
- [12] L. Talbot, R. K. Cheng, R. W. Schefer, and D. R. Willis. Thermophoresis of particles in a heated boundary layer. *Journal of Fluid Mechanics*, 101:737–758, 1980.

- [13] J. F. Richardson and W. N. Zaki. Sedimentation and fluidisation: Part one. *Trans. Inst. Chem. Eng.*, 32:35–53, 1954.
- [14] M. W. Rosenthal. Molten salt reactor program semi-annual progress report for pregiod ending august 31, 1967. Technical report ORNL-4191, Oak Ridge National Labortories, May 1967.
- [15] M. W. Rosenthal. Molten salt reactor program semi-annual progress report for pregiod ending february 29, 1968. Technical report ORNL-4254, Oak Ridge National Labortories, May 1968.
- [16] Nick Termini, Anthony Birri, Shane Henderson, and N. Dianne Bull Ezell. An overview of the molten salt thermal properties database—thermophysical, version 2.1.1 (mstdb-tp v.2.1.1). Technical report, Oak Ridge National Laboratory (ORNL), Oak Ridge, TN (United States), 2023.

DISTRIBUTION

Email—Internal

Name	Org.	Sandia Email Address
Technical Library	1911	sanddocs@sandia.gov



Sandia National Laboratories is a multimission laboratory managed and operated by National Technology & Engineering Solutions of Sandia LLC, a wholly owned subsidiary of Honeywell International Inc., for the U.S. Department of Energy's National Nuclear Security Administration under contract DE-NA0003525.